Research Article

Watermelon (*Citrullus lanatus*) Rind Extract-Mediated Synthesis of Manganese (II, III) Oxide Nanoparticles for Potential Theranostic Applications

Gelo P. Zaragosa, Carlo Nonato D. Ilem and Joel Garcia*
Department of Chemistry, De La Salle University, Manila, Philippines

* Corresponding author. E-mail: joel.garcia@dlsu.edu.ph DOI: 10.14416/j.asep.2024.02.002
Received: 1 November 2023; Revised: 6 December 2023; Accepted: 11 January 2024; Published online: 7 February 2024

Abstract
Plant extracts and microorganisms are widely utilized for the green synthesis of Mn_3O_4 nanoparticles. In this study, green synthesis of Mn_3O_4 nanoparticles for theranostic applications was performed using watermelon (*Citrullus lanatus*) rind extract as a reducing and stabilizing agent. The UV-visible absorption of the nanoparticles at 196 nm is associated with the surface plasmon resonance of Mn_3O_4 nanoparticles. FT-IR spectra presented the key chemical functional groups associated with the Mn–O vibrations and phytoconstituents of the watermelon rind extract. XRD analysis revealed the single-phase hausmannite crystalline structure of the Mn_3O_4 nanoparticles with an average crystallite size of 35.2 nm. SEM and TEM images of the synthesized Mn_3O_4 nanoparticles showed quasi-spherical shapes and a core size of 52.90 ± 8.19 nm and 35.89 ± 0.83 nm, respectively. EDS analysis indicated that the nanoparticles mainly comprised Mn, O, and C. Furthermore, the radical scavenging activity through the DPPH assay showed that the nanoparticles have significant antioxidant therapeutic potential, with an IC_{50} value of 20.62 ± 0.69 ppm. T_1 and T_2 relaxivities of Mn_3O_4 nanoparticles were 5.34 ± 0.11 $mM^{-1}s^{-1}$ and 63.47 ± 0.60 $mM^{-1}s^{-1}$, respectively, when measured at a clinically relevant field strength of 1.5 T, confirming their suitability as an MRI contrast agent for diagnostic imaging. These findings imply that the green synthesized Mn_3O_4 nanoparticles could be used as a theranostic agent for MRI applications.

Keywords: Antioxidant, Green synthesis, Mn_3O_4 nanoparticles, MRI contrast agent, Theranostics, Watermelon rinds

1 Introduction

Throughout the years, developing safer and more sustainable synthetic techniques has been an increasing interest in nanotechnology. Green chemistry is a discipline that aims to develop chemical products and processes that limit or even eliminate the use and production of hazardous substances. It also promotes waste reduction, minimization of consumption of energy and nonrenewable resources, and the creation of hazardous substances that are found to be detrimental to the environment [1]. Green chemistry is thus an alternative way of preparing materials and developing chemical processes that could prevent different detrimental effects on the environment, such as pollution.

In the literature, a variety of metal nanoparticles have already been synthesized using the methods of green chemistry. *Rubus rosifolius* Linn fruit extracts [2] and waste leather trimmings [3] were used to synthesize Ag nanoparticles and rice husk ash [4] was used to synthesize Zn-modified zeolite NaA. Meanwhile, it is of great interest to produce Mn_3O_4 nanoparticles in a green synthetic manner to promote green chemistry for sustainable development. Mn_3O_4 nanoparticles are recently used in many applications, such as an antimicrobial agent, electrochemical sensor, catalyst, and agricultural nano fertilizer. Several recent studies in the literature report that the green synthesis of Mn_3O_4 nanoparticles is particular to the bottom-up approach method commonly using different plant part extracts or certain microorganisms. One of the simplest, most cost-effective, and environmentally friendly green chemistry methods is using different plant extracts [5], [6]. Various plant extracts have been

successfully used in the green synthesis of Mn_3O_4 nanoparticles. Some of the plant extracts used were *Aspalathus linearis* leaves [7], *Azadirachta indica* leaves [8], *Costus woodsonii* flowers [9], *Phoenix dactylifera* date pits [10], *Olea ferruginea* leaves [11], *Eucalyptus robusta* and *Corymbia citriodora* leaves [12], and *Justicia adhatoda* leaves [13]. Meanwhile, an extensive literature review reveals that very few studies have been conducted to investigate the capabilities of agricultural wastes in synthesizing Mn_3O_4 nanoparticles. In the Philippines, watermelon rinds are being discarded and considered a major solid waste due to their unpleasant taste. However, the watermelon rind extract contains phytophenolic compounds such as polyphenols and flavonoids [14], which could mediate nanoparticle synthesis. Therefore, we hypothesized that watermelon rind extract could effectively synthesize Mn_3O_4 nanoparticles. In fact, several studies have already reported that watermelon rind extract was effective as a reducing and stabilizing agent for synthesizing various nanoparticles such as Fe_3O_4 and bimetallic Se-Ag for different target applications [15], [16].

Manganese oxide nanoparticles, like MnO_2 and Mn_3O_4, have recently gained attention as safer MRI T_1 or T_2 contrast agents. The utilization of the transition metal manganese as nanoparticles is considered promising due to them being highly biocompatible as they are an endogenous element, paramagnetic, and its reported lower toxicity than that of traditional materials used for T_1 imaging such as gadolinium-based complexes [17], [18]. Moreover, employing the green synthesis route in manganese oxide-based nanoparticles makes it even more promising due to its enhanced safeness. Currently, there are still no studies that report the use of plant-extract mediated synthesized Mn_3O_4 nanoparticles as MRI contrast agents. Here, we present the antioxidant properties and contrast-enhancing efficacy of greenly synthesized Mn_3O_4 nanoparticles.

2 Materials and Methods

2.1 *Preparation of the watermelon rind ethanolic plant extract*

Frozen watermelon rinds were subjected to freeze-drying for 3 days to obtain the crushed plant powder. The plant powder (50.2456 g) was mixed with 100 mL 60% ethyl alcohol solution and extracted for 24 h. The resulting mixture was then filtered, and the collected filtrate was used as the plant extract solution for the green synthesis of Mn_3O_4 nanoparticles.

2.2 *Synthesis of Mn_3O_4 Nanoparticles*

Mn_3O_4 nanoparticles were synthesized through a bottom-up approach precipitation method (Scheme 1). To make the manganese salt precursor solution (0.1 M), $MnCl_2 \cdot 4H_2O$ (2.0054 g) was dissolved in an ethyl alcohol solution (100 mL, 60% w/v). The precursor solution (100 mL) was then mixed with the previously prepared plant extract solution (100 mL). The pH of the resulting mixture was adjusted to pH 8.04 by dropwise addition of a 50% (w/v) NaOH solution using a buret. After pH adjustment, the solution was transferred into a three-necked round bottom flask and refluxed for 4 h. The precipitates were collected by centrifuging the reaction mixture at 10,000 rpm for 15 min at 4 °C. The centrifugation was repeated three times, with the final run washing with distilled water. To remove any leftover solvent, the paste-like product was freeze-dried for 3 days. The dried product was then pulverized and transferred into a pre-conditioned 30-mL porcelain crucible. Afterward, the product was calcined in a muffle furnace at 400 °C for 2 h. Finally, the powder product was stored in a 5 mL vial for surface modification (0.4514 g, yield = 88%).

2.3 *Surface modification of the synthesized nanoparticles with polyacrylic acid (PAA)*

Polyacrylic acid (PAA, 5% v/v) solution was prepared by mixing polyacrylic acid (20 mL) with distilled water (80 mL). To this solution was added the as-synthesized nanoparticle (1.0029 g), and the reaction mixture was stirred at 200 rpm at ambient temperature for 30 min, then heated to 75 °C for 4 h with vigorous stirring. After 4 h, the mixture was allowed to cool and then transferred into Corning tubes. The mixture was centrifuged at 10,000 rpm, 4 °C for 15 min to separate the coated nanoparticles. The supernatant was discarded, and the paste product was subjected to freeze-drying for 48 h to finally obtain the dark brown-colored PAA-coated nanoparticles (0.2392 g, yield = 53%).

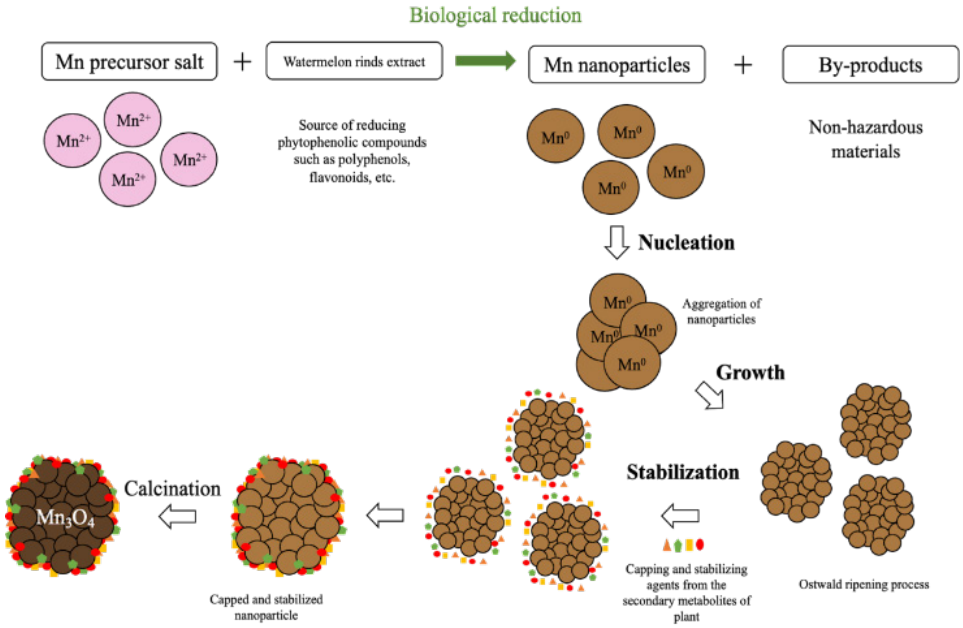

Scheme 1: Synthetic scheme of the manganese oxide nanoparticles capped with the phytophenolic compounds from watermelon rinds and surface modification with polyacrylic acid (PAA).

2.4 *Characterization of the PAA-coated Mn_3O_4 nanoparticles*

An ultraviolet-visible (UV-Vis) double-beam spectrophotometer (Hitachi U-2000) was employed to identify and monitor the surface plasmon resonance and stability of the nanoparticles. Fourier transform-infrared (FT-IR) spectra were obtained via the KBr pellet method of solid analyses operated on a spectrophotometer (Thermo Fisher Scientific Nicolet 6700) to determine the significant functional groups present on the pre– and post-modified nanoparticles. The surface morphology characterization of the nanoparticles was carried out using Field Emission Scanning Electron Microscopy (FESEM, JSM-IT500HR InTouchScopeTM) equipped with an Energy Dispersive Spectrometer (EDS, JEOL) for elemental characterization. The information on the nanoparticle size, together with its inner structure, was gathered using High Resolution Transmission Electron Microscopy (HRTEM, model no. JEOL JEM 1220). X-ray diffraction (XRD) analysis was carried out using an X-ray powder diffractometer (Shimadzu MAXima XRD700) equipped with Cu-Kα radiation (1.542 Å) to characterize the nanoparticles' crystal phase structure. Information on the zeta potential, the surface charge of the nanoparticles, and their hydrodynamic diameter and aggregation state was revealed through Dynamic Light Scattering (DLS, Malvern Zetasizer Nano ZSP) measurements.

2.5 *Antioxidant assay*

The antioxidant activity of the as-synthesized nanoparticles and the watermelon rind extract were investigated using the 1,1-diphenyl-2-picrylhydrazyl (DPPH) radical scavenging assay. This assay was performed in a dark room to prevent unnecessary light reactions. Ascorbic acid was used as the reference standard and positive control in the assay to ensure the effectiveness of the DPPH assay. The ethanolic extract of watermelon rinds used in the green synthesis of the nanoparticles was purified through a rotary evaporator at 40 °C and 80 rpm for 30 min until a paste-like consistency was achieved. This purified extract was then used to prepare the stock solution of watermelon rind for the assay. Stock solutions of 100 ppm of the ascorbic acid standard, nanoparticles, and ethanolic extract of watermelon rinds were prepared by dissolving 2.5 mg of the standard or the samples

in 0.5 mL of 0.1 M HCl and diluting with ethyl alcohol (99.99% purity) in a 25 mL volumetric flask. Meanwhile, a stock solution of 1 mM of DPPH was prepared by dissolving DPPH powder (9.85 mg) in ethyl alcohol (25 mL, 99.99% purity). All stock solutions were transferred to a 30 mL amber bottle covered with aluminum foil to prevent unnecessary light reactions.

The test solutions with varying concentrations (0, 10, 20, 30, and 40 ppm) of the standard and the samples were prepared using ethyl alcohol as the solvent. Finally, the prepared DPPH stock solution (80 µL) was added into each well, with a total volume of 200 µL in the 96-well flat-bottom microplate. The test solutions in the microplate were incubated in the dark for 30 min before the absorbance at 517 nm was measured using the FLUOstar Omega multimodal microplate reader (BMG LabTech). The radical scavenging activity (%RSA) was calculated using Equation (1).

$$\%RSA = \frac{Abs_{control} - Abs_{sample}}{Abs_{sample}} \times 100 \quad (1)$$

Following the determination of %RSA, the average %RSA values were plotted against the different concentrations to obtain the equation of the line with a desired R^2 value close to unity. The slope and y-intercept of the plot were used to calculate the half-maximal inhibitory concentration (IC_{50}) values of the standard and the samples, where b is the y-intercept and m is the slope of the line using Equation (2).

$$IC_{50} = \frac{50 - b}{m} \quad (2)$$

2.6 *Relaxivity measurements*

To investigate the contrast-enhancing efficiency of the as-synthesized nanoparticles, the T_1 and T_2 relaxation times of the as-synthesized nanoparticles were acquired using a 60 MHz benchtop NMR spectrophotometer (Nanalysis). Aqueous solutions of $MnCl_2 \cdot 4H_2O$ with different concentrations (0, 0.25, 0.50, 0.75, 1.0, and 1.5 mM) were prepared and transferred in separate NMR tubes. The samples in the NMR tubes were equilibrated with the temperature of the magnet of the benchtop NMR spectrophotometer in a sample warmer at 31.3 °C. The Mn concentration of each test solution was measured using an atomic absorption spectrophotometer (AA-6300 Shimadzu). The T_1 and T_2 relaxation times were measured using a spin-echo sequence with a pulse angle of 80.32°, scan delay of 1 s, and tau stop at 800 ms. Triplicate measurements were taken from the lowest concentration to the highest concentration. Finally, the reciprocal of the T_1 and T_2 values for each trial were plotted against the actual concentration of Mn to determine the longitudinal and transverse relaxivities, r_1 and r_2, respectively.

3 Results and Discussion

3.1 *Synthesis and Characterization of PAA-coated Mn_3O_4 Nanoparticles*

The mechanism of the formation of the manganese oxide nanoparticles through plant-mediated green synthesis involves the reduction of Mn^{2+} in the precursor salt solution through the phenolic compounds present in the plant extract, which possess hydroxyl and ketone groups [19] (Figure 1). These functional groups can bind to metal ions and reduce the metal ions to their zero-valent form. Subsequently, a nucleation process occurs, resulting in the clustering aggregation of the particles in the solution, which will eventually enter the growth stage of the nanoparticles due to the Ostwald ripening process. This process is thermodynamically spontaneous because larger-sized particles are more energetically favored than smaller particles. Finally, the secondary metabolites in the plant extract stabilize the outer surface of the resulting nanoparticles, defining their final morphological characteristics (i.e., size and shape). Upon calcination of these nanoparticles, manganese(II) oxide and manganese(III) oxide are formed, which grow as the hausmannite form of Mn_3O_4.

3.1.1 Optical property

The Mn_3O_4 nanoparticle formation was examined using UV-Vis spectroscopy. The spectra (Figure 2) of the as-synthesized nanoparticles showed a characteristic peak at 196 nm, mainly attributed to the localized surface plasmon resonance. In contrast, no significant peak was observed on the spectra of the precursor salt solution, clearly indicating nanoparticle formation. The obtuse absorption peak was most likely caused

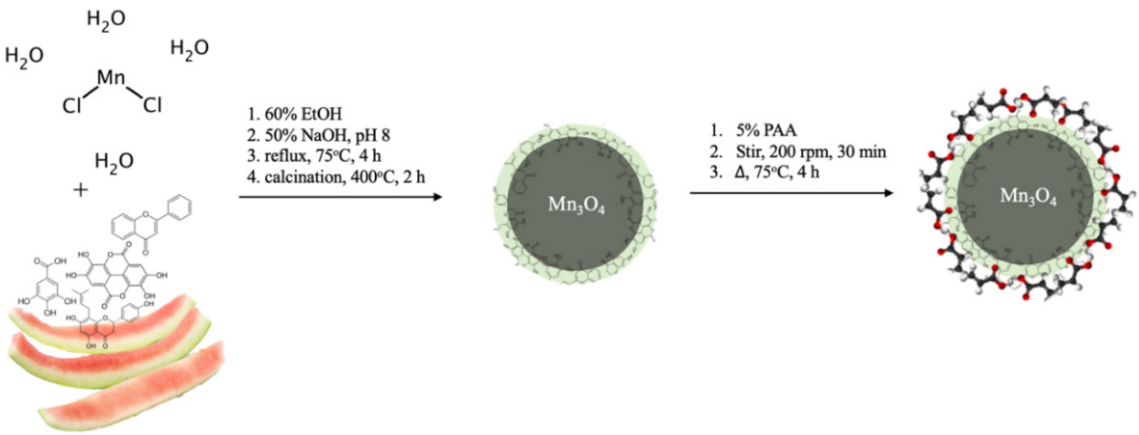

Figure 1: Formation mechanism of Mn_3O_4 nanoparticles using the plant extract-mediated synthesis method as discussed in the study of Prasad [13].

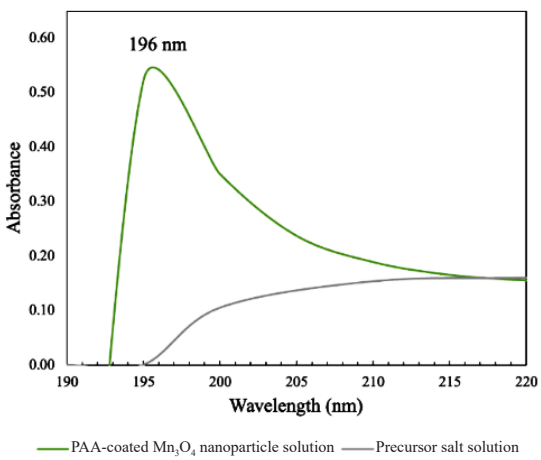

Figure 2: UV-Vis Spectra of the PAA-coated Mn_3O_4 nanoparticles (green) and the $MnCl_2 \cdot 4H_2O$ (gray) solution.

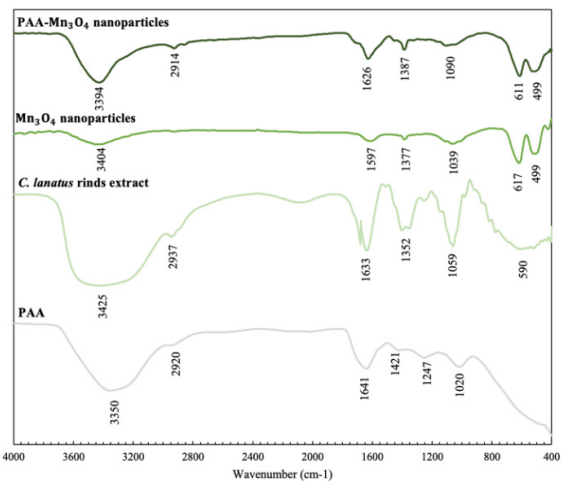

Figure 3: FT-IR Spectra of PAA (gray), watermelon rind extract (lightest green), pre- (lighter green), post-surface modified with PAA (dark green) Mn_3O_4 nanoparticles.

by the presence of PAA coating on the surface of the nanoparticle [20], suggesting that PAA was successfully coated on the nanoparticle.

3.1.2 Functional groups on the nanoparticle surface

The presence of substantial phytophenolic chemicals in the watermelon rind extract was confirmed by FT-IR data. The broad band at 3425 cm^{-1} corresponds to the rich hydroxyl O–H groups of the abundant polyphenols in the plant extract (Figure 3). The peak at 2937 cm^{-1} is attributed to C–H stretching vibrations of methyl and methoxy groups [21]. It also indicates that the rather sharp peak at 1633 cm^{-1} can be attributed to the C=O ketone groups of the abundant flavonoids in the plant extract. Lastly, the 1352 and 1059 cm^{-1} intense bands refer to the C–N stretching vibrations of aliphatic and aromatic amines and C–O stretching, respectively [22], which may be attributed to the other phytochemicals such as the secondary metabolites found in the plant extract.

The FT-IR spectrum of the pre-surface modified Mn_3O_4 nanoparticles was obtained to investigate the Mn–O bonding state and probe the presence of

the different phytophenolic compounds as natural capping agents. The spectra revealed several characteristic peaks in the lower frequency region, occurring between 400 and 650 cm^{-1}, which are associated with the vibration of the O–Mn–O bonds. The peak centered at 617 cm^{-1} is associated with the Mn^{2+}–O stretching modes found in tetrahedral sites. Furthermore, the peak at 499 cm^{-1} is attributed to the vibration of Mn^{3+} species in the octahedral sites. Other significant peaks, such as the characteristic band at 3404 cm^{-1}, corresponding to the rich hydroxyl O–H groups of the various phytophenolic compounds existing as capping agents of the nanoparticles, while the 1597 cm^{-1} peak is attributed to the existing Mn–O–H bonding. As for the post-surface modified Mn_3O_4 nanoparticles, the stronger absorption found at 1626 cm^{-1} is due to the carbonyl C=O bond stretching vibration of the added carboxylic acid from PAA. Finally, the existence of a jagged peak at approximately 2914 cm^{-1} is attributed to the stretching vibration of polymeric CH_2 groups, which corresponds to the spectra PAA as a reference. This serves as another evidence that the PAA coating is indeed present on the surface of the nanoparticle [23].

3.1.3 Structural, crystallographic, and phase identification analysis

A powder X-ray diffractometer was utilized to obtain the structural pattern of the greenly synthesized Mn_3O_4 nanoparticles (Figure 4). The XRD pattern revealed several noticeable reflection peaks, which are indexed to the crystalline structure of Mn_3O_4 by the Crystallography Open Database (COD) using the Match! software. Lattice parameters of greenly synthesized Mn_3O_4 nanoparticles were determined at a = 7.77 Å, b = 7.97 Å and c = 16.13 Å having a primitive unit cell and a space group m m m (47) with index lattice planes at (100), (101), (111), (200), (211), (202), (300), (311), (222), (230). These parameters suggest good consistency with a standard profile of a single-phase orthorhombic hausmannite Mn_3O_4 referencing JCPDS Card No. 96-101-1263 from the COD. No peaks from other phases were found, suggesting the high purity of the synthesized Mn_3O_4 nanoparticles. Based on full-width half maxima (FWHM), the crystallite size (D) was calculated according to the Debye–Scherer formula [(Equation (3)].

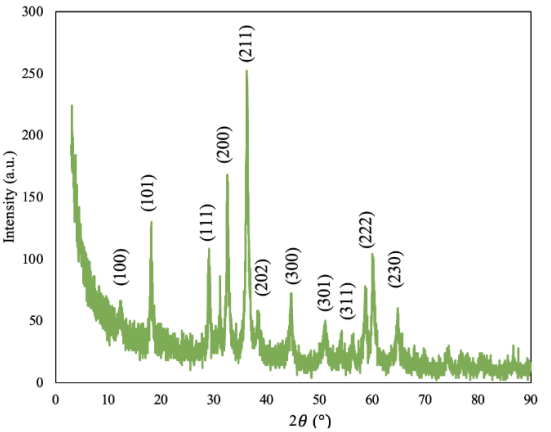

Figure 4: XRD profile of the PAA-coated Mn_3O_4 nanoparticles.

$$D = \frac{0.94\lambda}{\beta \cos\theta} \quad (3)$$

where λ is the wavelength (λ = 1.542 Å) (Cu-Kα), β is the FWHM of the line, and θ is the diffraction angle. The average crystallite size was estimated using the Debye-Scherer equation through the Match! Software, and it was found to be approximately 35.16 nm.

3.1.4 Electron microscopy morphological analysis

The general morphology, including the surface and nanostructures of the as-synthesized Mn_3O_4 nanoparticles, was confirmed by FE-SEM and HR-TEM data. From the low magnification FE-SEM image at 15,000x, as shown in Figure 5(a), it can be seen that the as-synthesized nanoparticles were highly dense and tended to aggregate into large clusters. This may be due to the strong interaction between the phytochemicals capped around the nanoparticles during the growth stage of the synthesis. Moreover, the magnification FE-SEM image at 70,000x, as shown in Figure 5(b), further revealed that the as-synthesized nanoparticles were irregularly shaped quasi-spherical forms. Lastly, at the magnification of 100,000x, as shown in Figure 5(c) and (d), the average size of the nanoparticles was measured and found to be 52.90 ± 8.19 nm.

On the other hand, HR-TEM has been utilized to further analyze the morphology of the as-synthesized Mn_3O_4 nanoparticles in great detail. Figures 6(a) and (b) confirm the quasi-spherical morphology obtained

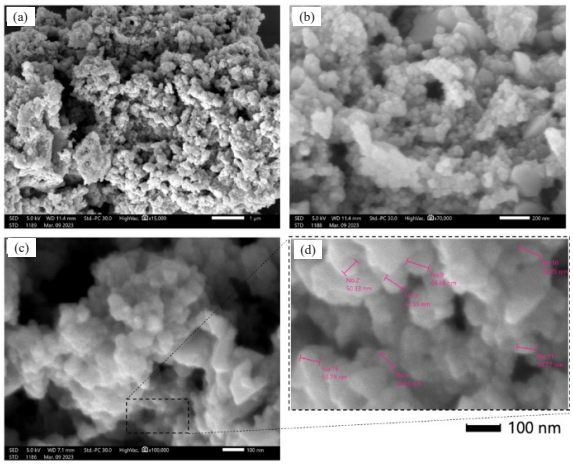

Figure 5: SEM microphotographs of the PAA-coated Mn_3O_4 nanoparticles showing clusters of quasi-spherical shapes at (a) 15,000x magnification; (b) 70,000x magnification; (c) 100,000x magnification; (d) with size measurement of the individual particles.

from FE-SEM analysis and a particle size ranging from 35.20 to 36.81 nm, also within the range of the obtained particle size in SEM imaging. Through the measured size of the individual particles in HR-TEM imaging, the green synthesized nanoparticles appeared to be a single crystalline in structure as the crystallite size of 35.16 nm estimated from the Debye-Scherrer formula in XRD profile analysis appeared to be relatively close to the measured size of in TEM. Furthermore, a compelling image of a single crystallized Mn_3O_4 nanoparticle shown in Figure 6(c) revealed that the particle is coated possibly with polyacrylic acid on top of the secondary metabolites of the watermelon rind as the capping and stabilizing agents, as depicted by a soft-like material around the outer surface of the particle.

3.1.5 Elemental analysis

The major elemental composition of the PAA-coated Mn_3O_4 nanoparticles was manganese (Mn), oxygen (O), and carbon (C) (Figure 7). The EDS spectrum shows the respective elemental peaks of Mn found at ~0.6, 5.8, and 6.4 keV, O at ~0.5 keV, and C at ~0.2 keV, which is attributed to optical absorption in the said regions due to the surface plasmon resonance (SPR) as shown in Figure 2. The C signal signifies that

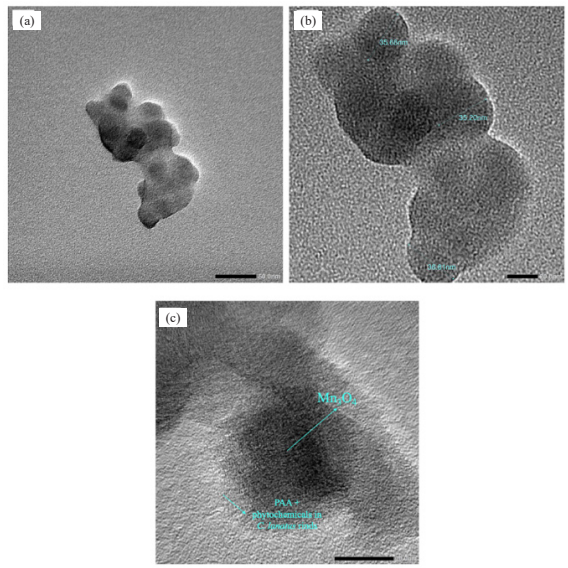

Figure 6: High-resolution transmission electron microscopy bright field (HR-TEM-BF) image of the PAA-coated Mn_3O_4 nanoparticles at (a) 100,000x, (b) 150,000x, and (c) 300,000x magnification showing a single crystallized Mn_3O_4 nanoparticles coated with PAA, and the secondary metabolites present in watermelon rinds.

the as-synthesized Mn_3O_4 nanoparticles have been successfully coated with the different phytophenolic compounds of the watermelon rinds and PAA from the surface modification. A platinum (Pt) signal was also detected, attributed to the platinum sputter coating applied to the nanoparticle for conductivity purposes using the SEM-EDS instrument.

3.2 *Antioxidant properties*

The DPPH radical scavenging assay was utilized to test the free-radical scavenging activity of the as-synthesized Mn_3O_4 nanoparticles in parallel with the watermelon rind extract used to greenly synthesize the nanoparticles. Antioxidants are chemical substances that can scavenge free radicals by transferring one electron from reactive oxygen species. The reducing ability of the antioxidants of as-synthesized Mn_3O_4 nanoparticles and watermelon rind extract was evaluated spectrophotometrically to monitor the antioxidant-induced decolorization of DPPH from violet to yellow color. The radical scavenging activity (%RSA)

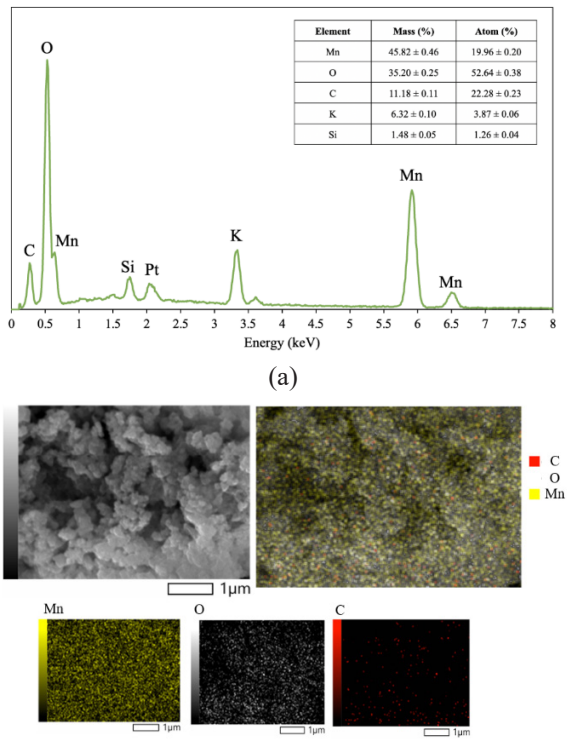

Figure 7: EDS point spectrum of the PAA-coated Mn_3O_4 nanoparticles.

and the half maximal inhibitory concentration (IC_{50}) were computed to compare the potency of the radical scavenging capabilities of the as-synthesized Mn_3O_4 nanoparticles to the watermelon rind extract.

Generally, lower IC_{50} values depict higher radical scavenging activity and, thus, better antioxidant properties. Figure 8 shows the effect of different concentrations on free-radical scavenging activities of the ascorbic acid standard, PAA-coated Mn_3O_4 nanoparticles, and the watermelon rind extract. This assay revealed that the PAA-coated Mn_3O_4 nanoparticles and the watermelon rind extract could act as a DPPH radical scavenger in a concentration-dependent manner. At 10–40 ppm concentrations, the nanoparticles exhibited a radical scavenging activity of 36–83%, while the watermelon rind extract had 27–67%. Meanwhile, the radical scavenging activity of the Mn_3O_4 nanoparticles was highest at low concentrations of 10 ppm. The radical scavenging activity of the nanoparticles rose by 82% as the

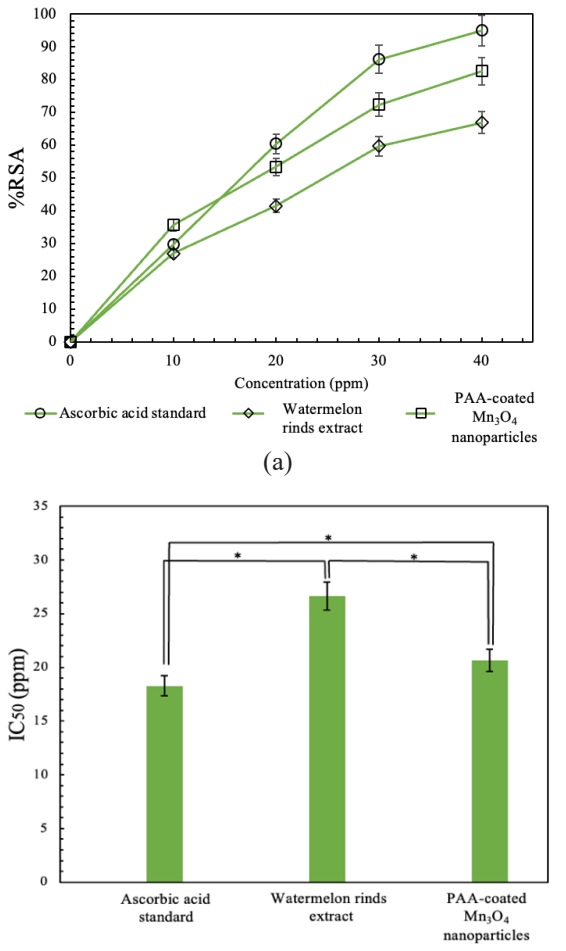

Figure 8: (a) DPPH antioxidant assay results show the effect of %RSA on different concentrations and (b) IC_{50} values for comparison with significant differences at a 95% confidence interval.

concentration increased from 0–40 ppm, but not as high as the ascorbic acid standard. The PAA-coated Mn_3O_4 nanoparticles also had a higher radical scavenging activity of about 20.74% in all concentrations than the watermelon rind extract used to prepare the nanoparticles. The IC_{50} values also demonstrate the antioxidant potencies of the samples. The ascorbic acid standard has the lowest IC_{50} value of 18.28 ± 0.16 ppm among the three. When the Mn_3O_4 nanoparticles and the watermelon rind extract were compared, the nanoparticles surprisingly had a lower IC_{50} value of 20.62 ± 0.69 ppm compared to the watermelon rind

extract, which had the highest IC_{50} value of 26.62 ± 0.41 ppm among the three. Based on the %RSA and IC_{50} values, the PAA-coated Mn_3O_4 nanoparticles had higher radical scavenging activity than the watermelon rind extract. Furthermore, statistical analysis using paired samples t-test suggested that the %RSA of the synthesized Mn_3O_4 nanoparticles and watermelon rind extract in different concentrations from 10–40 ppm are statistically different at a 95% confidence level (p-value < 0.05). This attested that the radical scavenging activity of the Mn_3O_4 nanoparticles is significantly higher than the watermelon rind extract. The DPPH assay demonstrated that watermelon rinds are an excellent source of phenolic and flavonoid compounds, which have been reported to be the phytochemicals generally responsible for antioxidant capacity. In this study, the greenly synthesized Mn_3O_4 nanoparticles from watermelon rind extract possessed antioxidant activity due to the capped phenolic compounds surrounding the surface of the nanoparticle. It is also possible that the redox potential of the Mn^{2+} species in the nanoparticle enhanced the radical scavenging activity of the nanoparticle. Furthermore, because the Mn^{2+} species can also act as a free radical scavenger, the Mn_3O_4 nanoparticles had higher antioxidant activity than the watermelon rind extract alone.

3.3 *Relaxometric properties*

As MRI detects the electromagnetic field of the water protons, the presence of magnetic nanoparticles shortens the relaxation time of the water protons nearby, thus improving the signal contrast between the surroundings and distant background in magnetic resonance images. Meanwhile, the T_1 longitudinal relaxivity and the T_2 transverse relaxivity, denoted as r_1 and r_2, respectively, reflect the contrast-enhancing efficiency of magnetic nanoparticles, such as manganese oxide nanoparticles. Relaxivity, in units of $mM^{-1}s^{-1}$, is the relaxation rate of protons when the concentration of the paramagnetic metal ion such as Mn in the nanoparticle solution is 1 mM.

Most clinically approved MRI contrast agents are either paramagnetic gadolinium ion complexes or superparamagnetic iron oxide (magnetite) particles that work as T_1 and T_2 contrast agents, respectively. Gadolinium-based contrast agents (GBCAs) are the most commonly used T_1 contrast agents that enhance the detection and differentiation of pathological lesions and visualize the vasculature in magnetic resonance imaging applications. When their relaxivity values were compared with the as-synthesized manganese oxide nanoparticles in this study, the manganese oxide nanoparticles demonstrated a higher T_1 relaxivity value (i.e., 14–27% higher) than the commercially available GBCAs (i.e., Dotarem®, Gadovist®, Magnevist®, Omniscan®, OptiMARK®, and ProHance®) (Table 1). The reported T_1 longitudinal and T_2 transverse relaxivity values are 5.34 ± 0.11 $mM^{-1}s^{-1}$ and 63.47 ± 0.60 $mM^{-1}s^{-1}$, respectively, indicating the ability of the as-synthesized Mn_3O_4 nanoparticles to enhance MRI contrast (Figure 9). The percent differences in the obtained relaxivity values of our Mn_3O_4 nanoparticles in this work compared to the other Gd and Mn-based contrast agents are presented in Tables 1 and 2, respectively. Overall, our as-synthesized manganese oxide nanoparticles have the potential to provide greater and enhanced positive contrast than the commercially available GBCAs. Furthermore, compared to earlier studies that used manganese oxide nanoparticles as T_1 contrast agents, our as-synthesized manganese oxide nanoparticles had much greater T_1 relaxivity values. We were able to accomplish a green synthesis of manganese oxide nanoparticles with a greater relaxivity value than those synthesized through chemical methods.

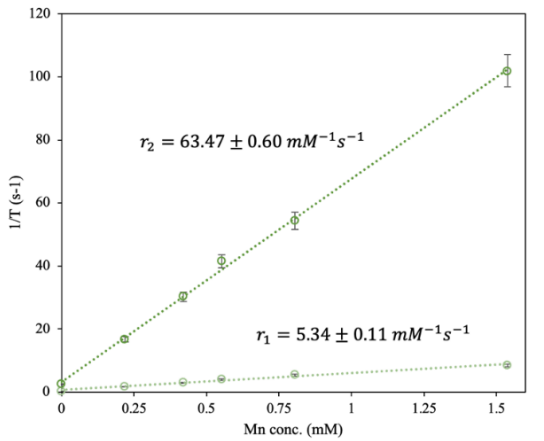

Figure 9: The linear plot obtained from the relaxivity measurements of the as-synthesized nanoparticles (equation of the lines: $1/T_1 = 5.34c_{Mn} + 0.66$, $R^2 = 0.9833$ and $1/T_2 = 63.47c_{Mn} + 3.24$, $R^2 = 0.9986$).

Table 1: Comparison of T_1 relaxivity values of reported Gd-based contrast agents at 1.5 T field strength [24]

Gd-based T_1 Contrast Agent	r_1 ($mM^{-1}s^{-1}$)	r_2/r_1	% Difference of r_1 with this work
Gd-DOTA (Dotarem®)	3.9 ± 0.2	1.19	27%
Gd-DO3A-butrol (Gadovist®)	4.6 ± 0.2	0.89	14%
Gd-DTPA (Magnevist®)	4.3 ± 0.4	1.13	19%
Gd-DTPA-BMA (Omniscan®)	4.5 ± 0.1	1.21	16%
Gd-DTPA-BMEA (OptiMARK®)	4.4 ± 0.2	1.11	18%
Gd-HP-DO3A (ProHance®)	4.4 ± 0.6	1.22	18%

Table 2: Comparison of T_1 and T_2 relaxivity values of reported Mn-based contrast agents at 1.5 T field strength

Mn-based Contrast Agent	r_1 ($mM^{-1}s^{-1}$)	r_2 ($mM^{-1}s^{-1}$)	r_2/r_1	% Difference	Ref
HMnO@ $mSiO_2$	1.72	11.28	6.56	68%, 82%	[25]
Amorphous hollow MnO	1.15	6.74	5.86	78%, 89%	[26]
Mn_3O_4 nanoplates	0.13	0.55	4.23	98%, 99%	[27]
PAA-Mn_3O_4	**5.34 ± 0.11**	**63.47 ± 0.60**	**12.08**		**This work**

The agglomeration of the PAA-coated Mn_3O_4 nanoparticles in this study, as seen in Figures 5 and 6, could pose significant drawbacks, particularly in the context of their application in MRI. Agglomeration leads to larger clusters, diminishing the nanoparticles' surface area, which is essential for effective interactions in MRI. Furthermore, the altered magnetic properties resulting from agglomeration can compromise the desired signal enhancement. Larger agglomerated nanoparticles may also experience reduced circulation times in the bloodstream, hindering their ability to navigate the vascular system and reach target tissues efficiently. To mitigate these challenges, strategies to reduce the agglomeration of Mn_3O_4 nanoparticles include surface modification through the introduction of repelling functional groups, ultrasonication to disperse agglomerates, optimization of synthesis conditions, controlled size synthesis, and the use of stabilizing agents such as surfactants or polymers. These approaches aim to enhance the stability and dispersibility of Mn_3O_4 nanoparticles, ensuring their optimal performance in MRI applications.

4 Conclusions

In this work, Mn_3O_4 nanoparticles were successfully synthesized using the phytophenolic compounds extracted from watermelon rinds for their potential as a theranostic agent. In addition to the naturally capped phytophenolic compounds around the nanoparticles, polyacrylic acid (PAA) coating was added as a surface modification to improve the hydrophilicity of the nanoparticles in aqueous dispersions. The synthesized nanoparticles exhibited profound radical scavenging activity with an IC_{50} value of 20.62 ± 0.69 ppm compared to the IC_{50} value of the watermelon rind extract, which was found to be 26.62 ± 0.40 ppm. Statistical analysis using paired samples t-test revealed that the antioxidant capability of the synthesized nanoparticles was significantly higher than the watermelon rinds. Also, relaxometric studies demonstrated that the synthesized nanoparticles are promising T_1 and T_2 contrast agents, having r_1 and r_2 values of 5.34 ± 0.11 $mM^{-1}s^{-1}$ and 63.47 ± 0.60 $mM^{-1}s^{-1}$, respectively, at a clinically relevant field strength (1.5 T) Our synthesized Mn_3O_4 nanoparticles possessed higher T_1 relaxivity values than the commercially available GBCAs and other reported Mn-based nanoparticles. Overall, the potential of the synthesized Mn_3O_4 nanoparticles for theranostic applications was demonstrated as an antioxidant therapeutic and an MRI T_1 contrast agent. Studies are underway exploring other applications and the molecular factors contributing to the superior relaxivity of the greenly synthesized Mn_3O_4 nanoparticles.

Acknowledgments

The authors are grateful to the Department of Chemistry, College of Science, De La Salle University (DLSU), DLSU Central Instrumentation Facility, and the University of the Philippines National Institute of Geological Sciences for their services provided for the various instrumentation analyses conducted in this work. Lastly, the authors acknowledge the institutions

financially supporting this work: the DLSU Office of the Vice Chancellor for Research and Innovation and the University Research Coordination Office (URCO).

Author Contributions

G.Z.: conceptualization, investigation, methodology, research design, data analysis, writing, reviewing, and editing; C.I.: conceptualization, investigation, data collection, analysis, writing, reviewing, and editing; J.G.: conceptualization, writing, reviewing, and editing, funding acquisition, project administration. All authors have read and agreed to the published version of the manuscript.

Conflicts of Interest

The authors declare no conflict of interest.

References

[1] P. C. Mishra and A. K. Giri, "Green Chemistry," in *Advances in Environmental Engineering and Green Technologies Book Series*. United States: Engineering Science Reference, 2018, pp. 152–161, doi: 10.4018/978-1-5225-3126-5.ch009.

[2] M. M. Martin and R. E. Sumayao Jr., "Facile green synthesis of silver nanoparticles using *Rubus rosifolius* Linn aqueous fruit extracts and its characterization," *Applied Science and Engineering Progress*, vol. 15, no. 3, 2021, Art. no. 5511, doi: 10.14416/j.asep.2021.10.011.

[3] B. Ashok, M. Umamahesh, N. Hariram, S. Siengchin, and A.V. Rajulu, "Modification of waste leather trimming with in situ generated silver nanoparticles by one step method," *Applied Science and Engineering Progress*, vol. 14, no. 2, pp. 236–246, Jan. 2021, doi: 10.14416/j.asep.2021.01.007.

[4] P. Tobarameekul, S. Sangsuradet, N. N. Chat, and P. Worathanakul, "Enhancement of CO_2 adsorption containing Zinc-ion-exchanged Zeolite NaA synthesized from rice husk ash," *Applied Science and Engineering Progress*, vol. 15, no. 1, Nov. 2020, Art. no. 3640, doi: 10.14416/j.asep.2020.11.006.

[5] M. Jayandran, M. Haneefa and V. Balasubramanian, "Green synthesis and characterization of Manganese nanoparticles using natural plant extracts and its evaluation of antimicrobial activity," *Journal of Applied Pharmaceutical Science*, vol. 5, no. 12, pp. 105–110, 2015, doi: 10.7324/JAPS.2015.501218.

[6] V. Hoseinpour, M. Souri, and N. Ghaemi, "Green synthesis, characterisation, and photocatalytic activity of manganese dioxide nanoparticles," *Micro & Nano Letters*, vol. 13, pp. 1560–1563, Nov. 2018, doi: 10.1049/mnl.2018.5008.

[7] A. Diallo, N. Tandjigora, S. Ndiaye, T. Jan, I. Ahmad, and M. Maaza, "Green synthesis of single phase hausmannite Mn_3O_4 nanoparticles via *Aspalathus linearis* natural extract," *SN Applied Sciences*, vol. 3, no. 562, Apr. 2021, doi: 10.1007/s42452-021-04550-3.

[8] J. K. Sharma, P. Srivastava, S. Ameen, M. S. Akhtar, G. Singh, and S. Yadava, "*Azadirachta indica* plant-assisted green synthesis of Mn_3O_4 nanoparticles: Excellent thermal catalytic performance and chemical sensing behavior," *Journal of Colloid and Interface Science*, vol. 472, pp. 220–228, Jun. 2016, doi: 10.1016/j.jcis.2016.03.052.

[9] T. V. Tran, D. T. Nguyen, P. S. Kumar, A. T. Din, A. S. Qazaq, and D.-V. N. Vo, "Green synthesis of Mn_3O_4 nanoparticles using *Costus woodsonii* flowers extract for effective removal of malachite green dye," *Environmental Research*, vol. 214, Nov. 2022, Art. no. 113925, doi: 10.1016/j.envres.2022.113925.

[10] J. Sackey, M. Akbari, R. Morad, A. K. H. Bashir, N. M. Ndiaye, N. Matinise, and M. Maaza, "Molecular dynamics and bio-synthesis of *Phoenix dactylifera* mediated Mn_3O_4 nanoparticles: Electrochemical application," *Journal of Alloys and Compounds*, vol. 854, Feb. 2021, Art. no. 156987, doi: 10.1016/j.jallcom.2020.156987.

[11] T. Zahra, K. S. Ahmad, C. Zequine, A. G. Thomas, M. A. Malik, R.K. Gupta, and D. Ali, "Preparation of organo-stabilized Mn_3O_4 nanostructures as an electro-catalyst for clean energy generation," *Journal of Electronic Materials*, vol. 50, pp. 5150–5160, Jul. 2021, doi: 10.1007/s11664-021-09054-9.

[12] J. P. Z. Gonçalves, J. Seraglio, D. L. P. Macuvele, N. Padoin, C. Soares, and H. G. Riella, "Green synthesis of manganese based nanoparticles

mediated by *Eucalyptus robusta* and *Corymbia citriodora* for agricultural applications," *Colloids and Surfaces A: Physicochemical and Engineering Aspects*, vol. 636, Mar. 2022, Art. no. 128180, doi: 10.1016/j.colsurfa.2021.128180.

[13] A. S. Prasad, "Green synthesis of nanocrystalline manganese (II, III) oxide," *Materials Science in Semiconductor Processing*, vol. 71, pp. 342–347, Nov. 2017, doi: 10.1016/j.mssp.2017.08.020.

[14] M. Mushtaq, B. Sultana, H. N. Bhatti, and M. Asghar, "RSM based optimized enzyme-assisted extraction of antioxidant phenolics from underutilized watermelon (*Citrullus lanatus* Thunb.) rind," *Journal of Food Science and Technology*, vol. 52, no. 8, pp. 5048–5056, Sep. 2014, doi: 10.1007/s13197-014-1562-9.

[15] C. Prasad, S. Gangadhara, and P. Venkateswarlu, "Bio-inspired green synthesis of Fe_3O_4 magnetic nanoparticles using watermelon rinds and their catalytic activity," *Applied Nanoscience*, vol. 6, pp. 797–802, Aug. 2015, doi: 10.1007/s13204-015-0485-8.

[16] A. H. Hashem, G. S. El-Sayyad, A. A. Al-Askar, S. A. Marey, H. AbdElgawad, K. A. Abd-Elsalam, and E. Saied, "Watermelon rind mediated biosynthesis of bimetallic selenium-silver nanoparticles: Characterization, antimicrobial and anticancer activities," *Plants*, vol. 12, no. 18, Sep. 2023, Art. no. 3288, doi: 10.3390/plants12183288.

[17] LTS Research Laboratories, "Safety Data Sheet: Manganese Oxide," 2015. [Online]. Available: https://www.ltschem.com/msds/Mn_3O_4.pdf

[18] J. Garcia, S. Liu, and A. Louie, "Biological effects of MRI contrast agents: Gadolinium retention, potential mechanisms, and a role for phosphorus," *Philosophical Transactions of the Royal Society A*, vol. 375, Nov. 2017, doi: 10.1098/rsta.2017.0180.

[19] J. Jeevanandam, A. Barhoum, Y. Chan, A. Dufresne, and M. Danquah, "Review on nanoparticles and nanostructured materials: History, sources, toxicity, and regulations," *Beilstein Journal of Nanotechnology*, vol. 9, no. 1, pp. 1050–1074, Apr. 2018, doi: 10.3762/bjnano.9.98.

[20] Z. Ni, Z. Wang, L. Sun, B. Li, and Y. Zhao, "Synthesis of poly acrylic acid modified silver nanoparticles and their antimicrobial activities," *Materials Science and Engineering: C*, vol. 41, pp. 249–254, Aug. 2014, doi: 10.1016/j.msec.2014.04.059.

[21] R. Lakshmipathy, B. Palakshi, N. C. Sarada, K. Chidambaram, and S. Khadeer, "Watermelon rind-mediated green synthesis of noble palladium nanoparticles: Catalytic application," *Applied Nanoscience*, vol. 5, no. 2, pp. 223–228, Apr. 2014, doi: 10.1007/s13204-014-0309-2.

[22] A. Asaikkutti, P.S. Bhavan, K. Vimala, M. Karthik, and P. Cheruparambath, "Dietary supplementation of green synthesized manganese-oxide nanoparticles and its effect on growth performance, muscle composition and digestive enzyme activities of the giant freshwater prawn Macrobrachium rosenbergii," *Journal of Trace Elements in Medicine and Biology*, vol. 35, pp. 7–17, May 2016, doi: 10.1016/j.jtemb.2016.01.005.

[23] L. M. Sanchez, D. A. Martin, V. A. Alvarez, and J. S. Gonzalez, "Polyacrylic acid-coated iron oxide magnetic nanoparticles: The polymer molecular weight influence," *Colloids and Surfaces A: Physicochemical and Engineering Aspects*, vol. 543, pp. 28–37, Apr. 2018, doi: 10.1016/j.colsurfa.2018.01.050.

[24] Y.Shen, F. L. Goerner, C. Snyder, J. N. Morelli, D. Hao, D. Hu, X. Li, and V. M. Runge, "T_1 relaxivities of gadolinium-based magnetic resonance contrast agents in human whole blood at 1.5, 3, and 7 T," *Investigative Radiology*, vol. 50, no. 5, pp. 330–338, May 2015, doi: 10.1097/rli.0000000000000132.

[25] E. Momin, J. Choi, K. Yuan, H. Zaidi, J. Kim, M. Park, N. Lee, M. T. McMahon, A. Quinones-Hinojosa, J. W. M. Bulte, T. Hyeon, and A. A. Gilad, "Mesoporous silica-coated hollow manganese oxide nanoparticles as positive T_1 contrast agents for labeling and mri tracking of adipose-derived mesenchymal stem cells," *Journal of the American Chemical Society*, vol. 133, no. 9, pp. 2955–2961, Feb. 2011, doi: 10.1021/ja1084095.

[26] K. An, S. G. Kwon, M. Park, H. B. Na, S.-I. Baik, J. H. Yu, D. Kim, J. S. Son, Y. W. Kim, I. C. Song, W. K. Moon, H. M. Park, and T. Hyeon, "Synthesis of uniform hollow oxide nanoparticles

through nanoscale acid etching," *Nano Letters*, vol. 8, no. 12, pp. 4252–4258, Nov. 2008, doi: 10.1021/nl8019467.

[27] W. Zhan, W. Zhan, H. Li, X. Xu, X. Cao, S. Zhu, J. Liang, and X. Chen, "In vivo dual-modality fluorescence and magnetic resonance imaging-guided lymph node mapping with good biocompatibility manganese oxide nanoparticles," *Molecules*, vol. 22, no. 12, p. 2208, Dec. 2017, doi: 10.3390/molecules22122208.